Human Molecular Genetics, 2015, Vol. 24, No. 9 2578–2593

doi: 10.1093/hmg/ddv021
Advance Access Publication Date: 28 January 2015
Original Article

ORIGINAL ARTICLE

The ciliogenic transcription factor Rfx3 is required for the formation of the thalamocortical tract by regulating the patterning of prethalamus and ventral telencephalon

Dario Magnani[1], Laurette Morlé[2], Kerstin Hasenpusch-Theil[1], Marie Paschaki[2], Monique Jacoby[3], Stéphane Schurmans[4], Bénédicte Durand[2] and Thomas Theil[1,*]

[1]Centre for Integrative Physiology, University of Edinburgh, Hugh Robson Building, Edinburgh EH8 9XD, UK, [2]Centre de Génétique et de Physiologie Moléculaires et Cellulaires, CNRS UMR 5534, Université Claude Bernard Lyon 1, Villeurbanne, Lyon F69622, France, [3]Institute of Immunology, Centre de Recherche Public de la Santé/ Laboratoire National de Santé, Luxembourg, Luxembourg and [4]Laboratory of Functional Genetics, GIGA-Signal Transduction, GIGA B34, Université de Liège, Liège B-4000, Belgium

*To whom correspondence should be addressed at: Centre for Integrative Physiology, University of Edinburgh, Hugh Robson Building, Edinburgh EH8 9XD, UK. Tel: +44 131 650 3721; Fax: +44 131 650 6527; Email: thomas.theil@ed.ac.uk

Abstract

Primary cilia are complex subcellular structures that play key roles during embryogenesis by controlling the cellular response to several signaling pathways. Defects in the function and/or structure of primary cilia underlie a large number of human syndromes collectively referred to as ciliopathies. Often, ciliopathies are associated with mental retardation (MR) and malformation of the corpus callosum. However, the possibility of defects in other forebrain axon tracts, which could contribute to the cognitive disorders of these patients, has not been explored. Here, we investigate the formation of the corticothalamic/ thalamocortical tracts in mice mutant for *Rfx3*, which regulates the expression of many genes involved in ciliogenesis and cilia function. Using DiI axon tracing and immunohistochemistry experiments, we show that some *Rfx3*$^{-/-}$ corticothalamic axons abnormally migrate toward the pial surface of the ventral telencephalon (VT). Some thalamocortical axons (TCAs) also fail to leave the diencephalon or abnormally project toward the amygdala. Moreover, the *Rfx3*$^{-/-}$ VT displays heterotopias containing attractive guidance cues and expressing the guidance molecules Slit1 and Netrin1. Finally, the abnormal projection of TCAs toward the amygdala is also present in mice carrying a mutation in the *Inpp5e* gene, which is mutated in Joubert Syndrome and which controls cilia signaling and stability. The presence of identical thalamocortical malformations in two independent ciliary mutants indicates a novel role for primary cilia in the formation of the corticothalamic/thalamocortical tracts by establishing the correct cellular environment necessary for its development.

Received: September 9, 2014. **Revised and Accepted:** January 21, 2015

Introduction

Primary cilia are complex subcellular organelles protruding from the cell surface, which mediate several sensory functions and are involved in regulating the cellular response to several signaling pathways and in particular to Sonic hedgehog (Shh) signaling (1). Moreover, primary cilia have important roles in human diseases, and defects in primary cilia formation and/or function underlie several human syndromes commonly referred to as ciliopathies (2,3). These disorders are associated with a large variety of manifestations that often include neurological features such as MR, but much less is known about the specific signaling pathways and the pathogenesis at the cellular and tissue level that ultimately result in neurological disease phenotypes (4,5).

A common feature of ciliopathies is malformations of the corpus callosum (CC) which as the major forebrain commissure provides the interhemic exchange of information between the two cortical hemispheres. While the significance of callosal abnormalities for the MR pathogenesis of ciliopathy patients remains unclear, this finding raises the possibility that other prominent axon tracts of the forebrain are affected in ciliopathies. To explore this, we here investigate the formation of the corticothalamic/thalamocortical tracts in two ciliary mouse mutants. The thalamocortical tract connects the dorsal thalamus with the cerebral cortex thereby conveying sensory information from the external environment to the cortex. The corticothalamic tract in turn sends processed sensory information back to the thalamus thereby providing the feedforward and feedback mechanisms essential in this processing unit (6). The formation of the thalamocortical tract requires a complex navigation of thalamocortical axons (TCAs) through the prethalamus and ventral telencephalon (VT), and involves several guidepost cues along the thalamocortical path that control the navigation of thalamic axons. Two populations of pioneer neurons are located in the prethalamus and the VT projecting their axons into the thalamus and providing scaffolds for TCAs growing into the prethalamus and across the diencephalic/telencephalic boundary, respectively (7–10). In addition, cells from the lateral ganglionic eminence (LGE) migrate into the medial ganglionic eminence (MGE) to form a permissive corridor and guide TCAs through the otherwise non-permissive MGE (11). These corridor cells also mediate the sorting of TCAs according to their rostral/caudal origin in the thalamus by expressing the Slit1 and Nestin1 guidance factors (12). Interestingly, the development of the VT and of the prethalamus, which provide these guidepost cues, is under the control of Shh signaling, raising the possibility that the formation of the thalamocortical tract might be affected in primary cilia mutants. However, this has not been explored yet.

RFX transcription factors have been shown to play fundamental roles in ciliogenesis by regulating the expression of genes involved in cilia assembly or function (13–15). Accordingly, *Rfx3*-deficient mouse mutants exhibit several hallmarks of ciliopathies, in particular left–right asymmetry defects and hydrocephalus (13,14), yet importantly they survive until birth, providing a rare opportunity to study the formation of forebrain axon connections in a cilia mouse mutant. Indeed, the *Rfx3* mutation interferes with the formation of the CC (16). Here, we investigate the formation of the corticothalamic/thalamocortical tracts in *Rfx3*-deficient mice. In these animals, some corticothalamic axons (CTAs) abnormally migrate toward the amygdala. Moreover, only a small proportion of TCAs reach the dorsal telencephalon but many fail to migrate through the prethalamus, whereas others enter the VT but subsequently project ventrally toward the amygdala. These defects correlate with abnormal patterning of the prethalamus. In addition, the rostroventral telencephalon forms neural heterotopias at its pial surface containing a mixture of MGE- and LGE-derived cells expressing the Slit1 and Nestin1 guidance molecules. Finally, the abnormal ventral deflection of TCAs toward the amygdala is also found in a second ciliary mouse mutant, which is deficient for *Inpp5e*, a Joubert syndrome disease gene. Taken together, these analyses indicate a novel role for primary cilia in the development of thalamocortical tract.

Results

Rfx3$^{-/-}$ mutant embryos display defects in the development of thalamocortical connections

Recently, we showed that the ciliogenic transcription factor *Rfx3* is required for CC development (16). Here, we investigate whether an *Rfx3* null mutation also affects the formation of the thalamocortical/corticothalamic tracts. TCAs progress in a multistep fashion over their intermediate territories, the diencephalon and the VT (17). Thalamic neurons send their axons ventrally through the prethalamus toward the diencephalic–telencephalic boundary. After entering the telencephalon at E13.5, thalamic axons migrate through the VT via the internal capsule (ic) to reach the pallial–subpallial boundary (PSPB) and finally enter the cortical intermediate zone at E14.5. CTAs leave the cortex at around E14.5 and follow the same trajectory through the VT as TCAs but in the opposite direction. This trajectory is revealed in E18.5 control embryos by placement of DiI crystals into the cortex. This analysis also reveals the path of TCAs by retrograde labeling (Fig. 1A–D). *Rfx3*$^{-/-}$ mutant brains show a similar labeling pattern; however, we noted a number of backlabeled nuclei in the rostroventral telencephalon close to a region of the VT containing a heterotopia. This analysis also revealed an abnormal ventral projection toward the amygdala at intermediate and caudal levels (Fig. 1E–H). To more specifically label TCAs, we placed DiI crystals into the thalamus. TCAs are highly fasciculated in the ic, are arranged in roughly parallel bundles in the striatum and reach the cortex (Fig. 1I and J). In contrast, in *Rfx3*$^{-/-}$ mutant brains, thalamic axons appear disorganized in the striatum with some axons projecting toward the PSPB in more ventral regions (Fig. 1M and N). At caudal levels, TCAs abnormally project into the VT toward the amygdala similar to our findings on the CTA trajectory.

Immunostaining for the panaxonal marker Neurofilament (NF) confirmed the pathfinding defects revealed by DiI labeling. In control embryos, this analysis showed parallel organized axons in the thalamus, prethalamus, ic, the striatum and in the intermediate zone of the cerebral cortex (Fig. 1K and L). In *Rfx3*$^{-/-}$ mutants, NF staining revealed several abnormal fiber tracts. Many axons are already disorganized in the thalamus, and the exit and entry zones of CTAs and TCAs into and out of the cortex appear broader (Fig. 1O, arrowheads). Many NF^{+} fibers ectopically project toward the amygdala forming a highly fasciculated axon bundle at more caudal levels (Fig. 1P, arrow).

To gain insights into the origin of these axonal defects, we performed NF immunofluorescence analyses and DiI labeling on E14.5 control and *Rfx3*$^{-/-}$ mutant brains. At this stage, NF labels axons in the developing thalamus, prethalamus and VT of control embryos (Supplementary Material, Fig. S1A and B). The ic contains highly fasciculated NF^{+} axons, whereas axons are more loosely organized in the striatum (Supplementary Material, Fig. S1C and D). In *Rfx3*$^{-/-}$ embryos, NF^{+} axons are disorganized in the VT projecting in several directions within the LGE and MGE,

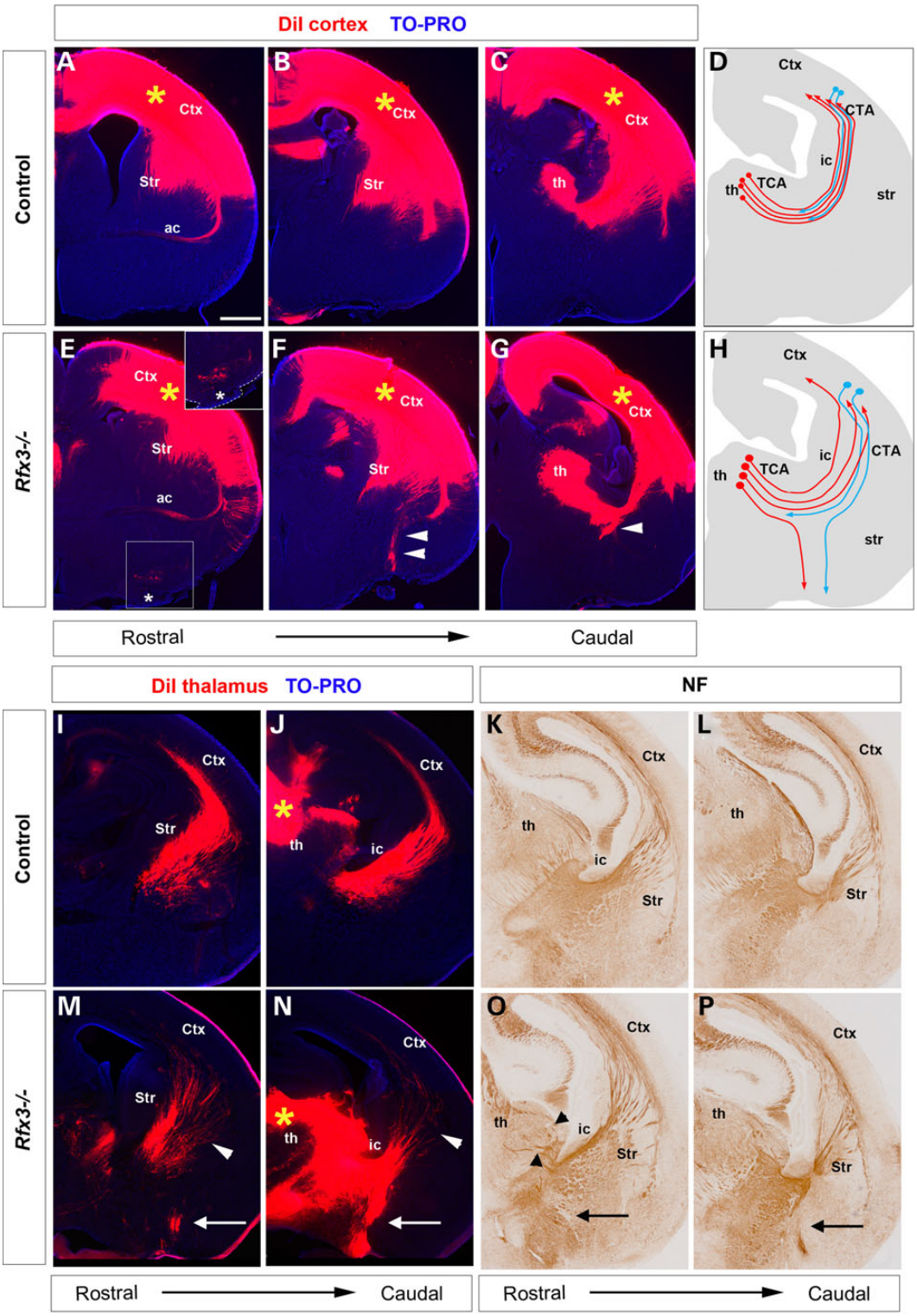

Figure 1. Axon guidance defects in the E18.5 *Rfx3*$^{-/-}$ brains. Coronal sections through the brain of control (**A–C** and **I–L**) and *Rfx3*$^{-/-}$ (**E–G** and **M–P**) E18.5 embryos. (A–C and E–G) DiI placements in the cortex (asterisks) reveal the anterior commissure (ac) (A and E) and the corticothalamic and thalamocortical tract through anterograde and retrograde labeling, respectively. In *Rfx3*$^{-/-}$ mutants, both tracts are formed but note the backlabeled neurons close to a heterotopia at the ventral telencephalic surface (inset and white asterisks in E) and the abnormal projections toward the amygdala at intermediate and caudal levels (arrowheads in F and G). (I, J, M and N) Thalamic DiI labeling (asterisks) revealed the TCA trajectory in control embryos (I and J). In *Rfx3*$^{-/-}$ mutants, TCAs cross the PSPB in a broader entry zone (arrowheads in M and N). Several axons leave the ic prematurely and form an ectopic axon bundle running ventrally toward the pial surface (arrows in M and N). (K, L, O and P) Immunostainings for NF showed axonal pathfinding defects in the diencephalon (arrowheads in O) and an ectopic axon bundle running ventrally toward the amygdala of *Rfx3*$^{-/-}$ embryos (arrows in O and P). (D and H) Schematic drawings summarizing the CTA and TCA pathfinding defects in *Rfx3*$^{-/-}$ mutants. Scale bar: 100 µm.

and a thick axon bundle runs ectopically toward the pial surface (Supplementary Material, Fig. S1F and G, arrow), whereas caudally no axons reached the PSPB (Supplementary Material, Fig. S1H and I). In addition, several NF$^+$ axons mis-project in the prethalamus resulting in the formation of abnormal bundles (Supplementary Material, Fig. S1I). These findings were confirmed by DiI labeling experiments of TCAs. In contrast to control embryos, very few TCAs traverse the VT with no axons reaching the PSPB in *Rfx3*$^{-/-}$ mutants (Supplementary Material, Fig. S1K, L and Q), but a large fiber bundle abnormally projects ventrally toward the telencephalic pia (Supplementary Material, Fig. S1R). To further dissect the path of thalamic axons, we performed calretinin (CR) immunofluorescence analysis. In control brains, CR selectively labels the first thalamic axons entering the VT and projecting through the ic (11) (Supplementary Material, Fig. S1O and P). In *Rfx3*$^{-/-}$ mutants, CR$^+$ axons were detected in the ic at rostral levels (Supplementary Material, Fig. S1U) but consistent with the NF immunostaining and DiI labeling experiments, many CR$^+$ axons migrated ventrally toward the pial surface after entering the VT at caudal levels (Supplementary Material, Fig. S1V). Also, some CR$^+$ axons form abnormal clusters in the thalamus. Finally, placing DiI crystals into the cortex revealed CTAs in control embryos having penetrated into the VT and retrogradely labeled neurons in the thalamus (Supplementary Material, Fig. S1M and N). In *Rfx3*$^{-/-}$ mutants, backlabeled neurons were not observed, instead a large axon bundle projects from the cortex toward the pia of the VT (Supplementary Material, Fig. S1S and T). Collectively, these analyses indicate severe disruptions in the *Rfx3*$^{-/-}$ corticothalamic/thalamocortical tracts, with many *Rfx3*$^{-/-}$ thalamic axons being misrouted in the prethalamus and VT.

Rfx3$^{-/-}$ mutants display abnormalities in the patterning of the prethalamus

From E9.5, *Rfx3* is expressed throughout the forebrain (16) including the cortex and thalamus where corticothalamic and thalamocortical neurons are born, respectively, and the prethalamus and VT through which CTAs and TCAs migrate. Therefore, the CTA/TCA pathfinding errors in *Rfx3*$^{-/-}$ mutants could result from defects in all three tissues. To start to identify the tissue (s) primarily responsible for the TCA phenotype, we first investigated the development of the *Rfx3*$^{-/-}$ mutant thalamus. To this end, we examined the expression of several transcriptional regulators including *Lhx2*, *Gbx2* and *Ngn2* that play key roles in specifying thalamic nuclei and in determining their axonal projection patterns (18–20). We also analyzed neuronal differentiation markers (Tuj1 and CR) and the expression of the axon guidance receptors *Robo1/2* (21). Overall, these analyses showed no obvious defects in the development of the *Rfx3*$^{-/-}$ thalamus which could explain the TCA guidance mistakes (Supplementary Material, Figs S2 and S3). Furthermore, we have previously shown that cortical lamination is not affected in *Rfx3*$^{-/-}$ mutants (16). We therefore focused our further analyses on the development of the prethalamus and VT starting with the prethalamus.

Since development of the prethalamus is controlled by Shh signaling from the zona limitans intrathalamica (zli) (22–25) and since primary cilia are crucial for Shh signaling, we first investigated *Shh* expression and that of its target genes *Ptc1* and *Gli1* in the *Rfx3*$^{-/-}$ diencephalon. This analysis did not reveal obvious defects in *Shh* zli expression (Fig. 2A, D and G), whereas the expression domains of *Ptc1* and *Gli1* appear expanded in the prethalamus but no significant changes were found in the expression levels of these genes as shown by qRT-PCR (Fig. 2B, C, E, F, H and I). Next, we investigated prethalamic patterning. In E14.5 control embryos, the prethalamic progenitor domain is characterized by Nkx2.2 expression (25) (Fig. 3A and B). This expression domain is expanded in *Rfx3*$^{-/-}$ mutants (Fig. 3C and D). Olig2, another marker for diencephalic progenitor cells, displays a more complex expression pattern. Immunofluorescence analysis showed a high-level Olig2 expression domain in prethalamic progenitors, and lower-level expression in thalamic progenitors, with a high^{ventral} to low^{dorsal} expression gradient (Fig. 3E, F, I and J). In the *Rfx3*$^{-/-}$ mutant diencephalon, the dorsal thalamic expression of Olig2 and its expression gradient is maintained (Fig. 3G, H, K and L). However, Olig2 expression is expanded in the prethalamus of *Rfx3*$^{-/-}$ mutants (Fig. 3H and L). Finally, the expression domain of the Pax6 transcription factor normally extends ventrally from the zli encompassing progenitors from the prethalamus and from the eminentia thalami, thereby delineating the boundary between the thalamus and prethalamus (Fig. 3E, F, I and J). In the *Rfx3*$^{-/-}$ mutants, Pax6 expression is maintained in prethalamic progenitors, but its expression in the diencephalic mantle is reduced (Fig. 3G, H, K and L). Taken together, these results suggest regionalization defects in the prethalamus of the *Rfx3*$^{-/-}$ mutants.

Abnormal MGE development and formation of heterotopias in the *Rfx3*$^{-/-}$ VT

Since *Rfx3*$^{-/-}$ mutants show several corticothalamic/thalamocortical pathfinding defects in the VT, we next investigated its development. Recently, we reported a slight down-regulation of Shh signaling in the MGE of *Rfx3*$^{-/-}$ mutants using *in situ* hybridization (16), but qRT-PCR showed no effect on *Shh* and *Gli1* expression, whereas *Ptc1* expression was mildly up-regulated ($P = 0.0384$; $n = 6$; Supplementary Material, Fig. S4). Correct levels of Shh signaling are crucial for establishing the PSPB separating the dorsal telencephalon and VT. However, expression analyses for *Dlx2*, Gsh2, Pax6 and *Dbx1* did not reveal abnormalities at this boundary (Fig. 4A and E, and Supplementary Material, Fig. S5). We next analyzed the subdivision of the VT into the MGE and LGE. *Dlx2* is expressed throughout the proliferative zone of the VT, whereas *Nkx2.1* expression is restricted to the MGE (Fig. 4A and B). Moreover, *Nkx6.2* expression is confined to progenitors on either side of the interganglionic sulcus (Fig. 4C). In *Rfx3*$^{-/-}$ embryos, these expression patterns are maintained except for a slight *Nkx6.2* down-regulation (Fig. 4E–G). We also noted an ectopic accumulation of *Dlx2* and *Nkx2.1* expressing cells outside the VT at its ventral surface (Fig. 4E–G) reminiscent of the heterotopia we observed at E18.5 (Fig. 1E). These heterotopias were detected on both sides of the rostral telencephalon in all *Rfx3* mutants but not in more caudal regions. Also, they varied in size with some extending toward the midline, whereas others were confined to the surface of the ventrolateral telencephalon. In addition, the heterotopias contain a mixture of progenitor cells and neurons. Expression of the MGE-specific genes *Lhx6* and *Lhx7*, which regulate *Shh* expression in the MGE and which are in turn Shh target genes (26), was detected in the heterotopias (Fig. 4H and M) as well as that of Tuj1 characteristic of differentiating neurons (Fig. 4N). Tuj1 immunofluroescence also showed a size reduction of the MGE mantle. Finally, we investigated whether disruption of the basal lamina, which normally surrounds the telencephalon, could account for heterotopia formation. Laminin immunofluorescence showed that the basal lamina is disrupted in several positions at the ventral pial surface of E12.5 and E14.5 *Rfx3*$^{-/-}$ mutants (Fig. 4O and P). Taken together, these analyses show a size reduction of the MGE mantle and a disruption of the basal

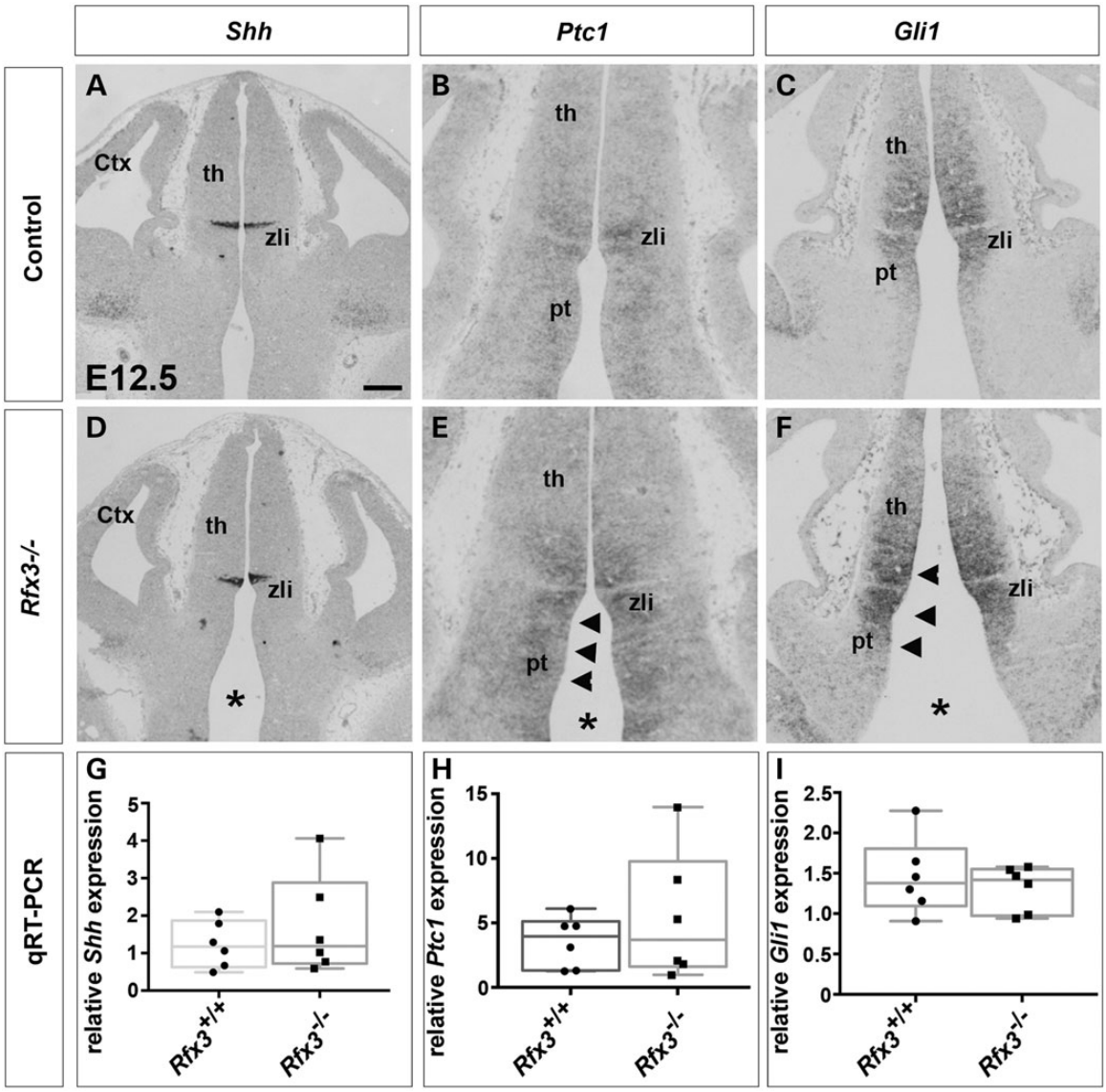

Figure 2. Shh signaling in *Rfx3*$^{-/-}$ mutant diencephalon. Coronal sections through the diencephalon of E12.5 control (**A–C**) and *Rfx3*$^{-/-}$ mutant embryos (**D–F**) hybridized with the indicated probes. (A and D) No major differences are observed in *Shh* expression in the *Rfx3*$^{-/-}$ zli compared with control embryos. Note the enlargement of the third ventricle in mutant embryos (asterisks in D, E and F). (B and C) *Ptc1* and *Gli1* are expressed in the diencephalon of control brains, but not in the zli. (E and F) Expanded expression of both *Ptc1* and *Gli1* is found in the prethalamus of *Rfx3*$^{-/-}$ mutants (arrowheads in E and F). (**G–I**) Quantification of *Shh* (G), *Ptc1* (H) and *Gli1* (I) expression in the diencephalon using qRT-PCR revealed no significant changes in the expression levels of these markers ($n = 6$). Scale bar: 100 µm.

lamina concomitant with the formation of neural heterotopias in *Rfx3*$^{-/-}$ embryos.

Cellular and molecular guidance cues are affected in the VT of *Rfx3*$^{-/-}$ embryos

Given these defects in the formation of the VT, we next analyzed whether ventral telencephalic guidance cues essential for TCA projection are also affected. Pioneer neurons located in the rostral MGE extend their axons into the thalamus and serve as scaffolds to guide TCAs across the diencephalic–telencephalic boundary (7–9). Since no markers are available to selectively label these MGE pioneer neurons, we investigated their formation by DiI placement into the E12.5 thalamus. In control embryos, these placements retrogradely labeled the pioneer axons and their cell bodies located in the rostral MGE (Fig. 5A and B). While this analysis also revealed pioneer neurons cell bodies and axons in the MGE mantle of *Rfx3*$^{-/-}$ mutants, their distribution appeared less dense (Fig. 5C and D). In addition, some DiI-labeled cell bodies were located in the heterotopic tissue outside the MGE mantle.

In addition to the MGE pioneer neurons, neurons derived from the LGE migrate into the MGE and form a corridor along which TCAs project through the otherwise non-permissive environment of the MGE. In control E12.5 and E14.5 brains, these guidepost cells are marked by both *Ebf1* and Islet1/2 expression from their origin in the LGE and during their migration into the MGE, where they form the ic (Fig. 6A–C). In E12.5 and E14.5 *Rfx3*$^{-/-}$ embryos, *Ebf1*-expressing cells originate normally in the LGE and migrate toward the MGE forming the corridor at caudal levels (Fig. 6F). However, at rostral levels, *Ebf1*-expressing cells migrate toward the heterotopias thereby abnormally connecting the

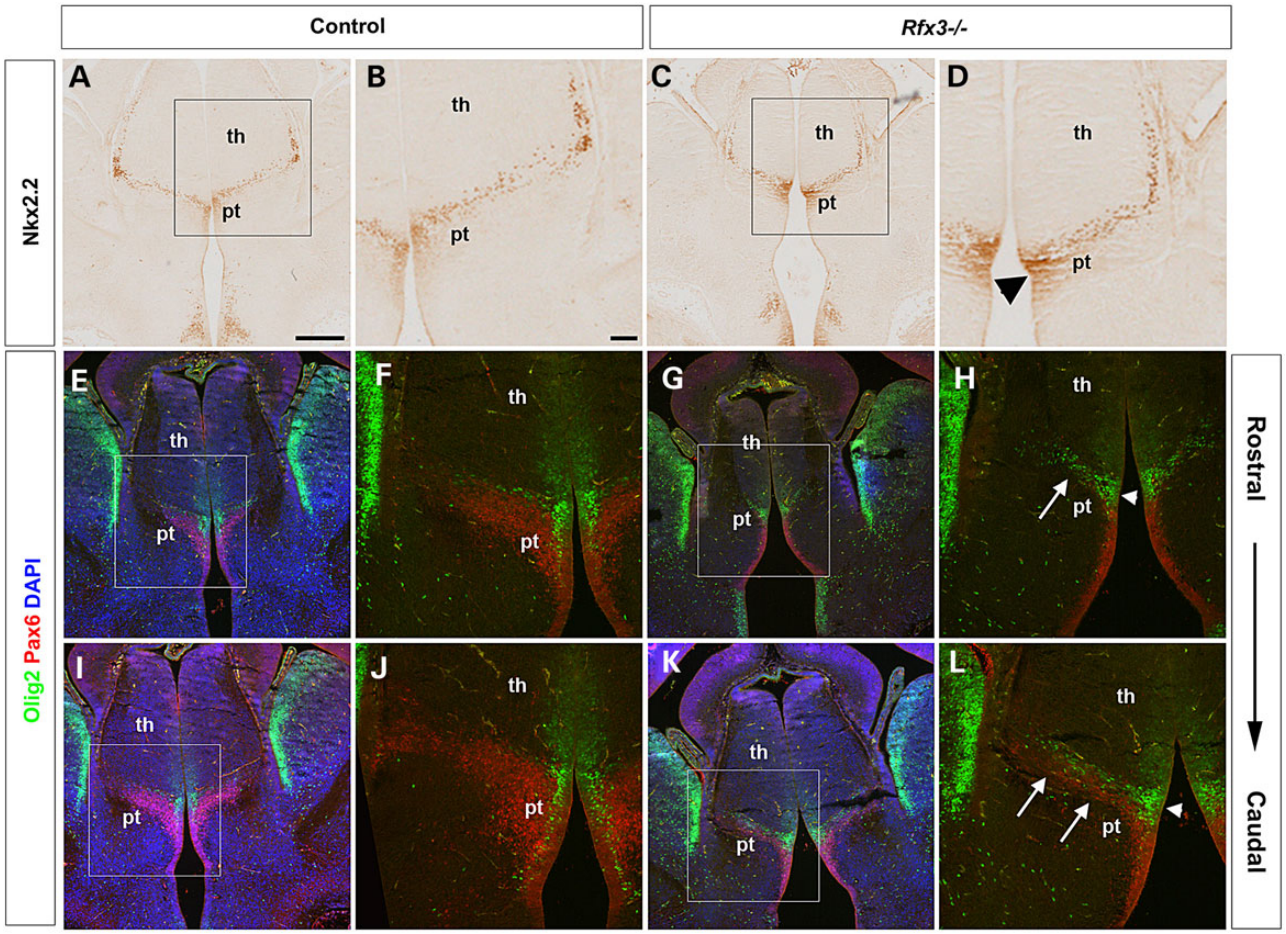

Figure 3. Patterning defects in the prethalamus of *Rfx3*$^{-/-}$ mutant brains. (**A–L**) Coronal sections through the diencephalon of E14.5 control (A, B, E, F, I and J) and mutant (C, D, G, H, K and L) brains were stained with the indicated antibodies. B, D, F, H, J and L are higher magnifications of A, C, E, G, I and K, respectively. (A and B) Nkx2.2 immunostaining labels the prethalamic progenitor domain. (C and D) Nkx2.2 expression was expanded in the diencephalon of *Rfx3*$^{-/-}$ mutants (arrowhead in D). (E, F, I and J) In control brains, Olig2 displays a high expression domain in the prethalamic progenitor region and is also detected at lower levels in the progenitor domain of the dorsal thalamus. (G, H, K and L) In the *Rfx3*$^{-/-}$ diencephalon, the dorsal thalamic expression of Olig2 and its gradient are maintained; however, the Olig2 prethalamic expression is expanded (arrowhead in H and L). (E, F, I and J) Pax6 is highly expressed in the diencephalon of control brains at the boundary between prethalamus and dorsal thalamus. (G, H, K and L) In the *Rfx3*$^{-/-}$ diencephalic ventricular zone, the Pax6 expression domain in the diencephalic mantle is reduced (arrows in H and L). Scale bars: 100 µm.

surface of the MGE mantel with the LGE (Fig. 6D and E). These abnormalities were confirmed by immunostainings for Isl1/2. As in control embryos, Isl1/2^{+} cells normally populate the corridor (Fig. 6G, H, J and K), but were also found ectopically in the heterotopic tissue in *Rfx3*$^{-/-}$ embryos (Fig. 6J and K). Finally, *Nkx2.1* expression labels the MGE ventricular zone and the globus pallidus of E14.5 control embryos, whereas the ic remains *Nkx2.1* negative (Fig. 6I). The *Nkx2.1* expression pattern in the *Rfx3*$^{-/-}$ MGE mantle appears unaltered in *Rfx3* mutants but as with the corridor markers, *Nkx2.1*-expressing cells were also detected in the ectopic tissue (Fig. 6L). These findings suggest that the MGE corridor forms at caudal levels, but that corridor cells abnormally migrate toward the heterotopias at rostral levels.

Next, we investigated whether the defects in forebrain patterning and in the formation of cellular guidance cues correlate with altered expression patterns of axon guidance molecules. Interestingly, *Sema6a*$^{-/-}$ mice show a very similar thalamocortical pathfinding defect as *Rfx3*$^{-/-}$ mutants with TCAs being deflected toward the amygdala after entering the VT (27). *Sema6a* has a highly complex expression pattern in the developing forebrain. Rostrally, *Sema6a* expression was mainly confined to the ventricular zone of the VT, but weak expression was also found in the heterotopias of *Rfx3*$^{-/-}$ embryos (Fig. 7A and E). Caudally, *Sema6a* transcripts were detected in thalamic neurons and in groups of cells along the path of TCAs in the prethalamus and dorsally and ventrally to the permissive corridor. This expression pattern is not affected by the *Rfx3* mutation (Fig. 7B and F). *PlexinA4* encodes a semaphorin receptor, and groups of *PlexinA4*-expressing cells delineate the corridor ventrally and dorsally and also reside in the caudal VT where TCAs normally not project (Fig. 7C and D). In *Rfx3*$^{-/-}$ embryos, *PlexinA4* expression largely persists in cells surrounding a smaller ic at rostral levels and in cells in the caudal VT where it is, however, adjacent to an ectopic axon bundle likely containing TCAs which mis-project toward the amygdala (Fig. 7G and H). *Sema5b* encodes a chemorepellent for corticofugal axons, and is expressed in telencephalic progenitor cells and in neurons of the piriform cortex. This expression pattern is maintained in *Rfx3*$^{-/-}$ embryos with no *Sema5b* expression in the heterotopias (Fig. 7I, J, M and N). We also investigated expression of *Netrin1* and *Slit1* which interact in the rostral/caudal sorting of TCAs in the corridor (12). In addition, *Slit1* regulates the migration of corridor cells in the MGE (28). Both genes are

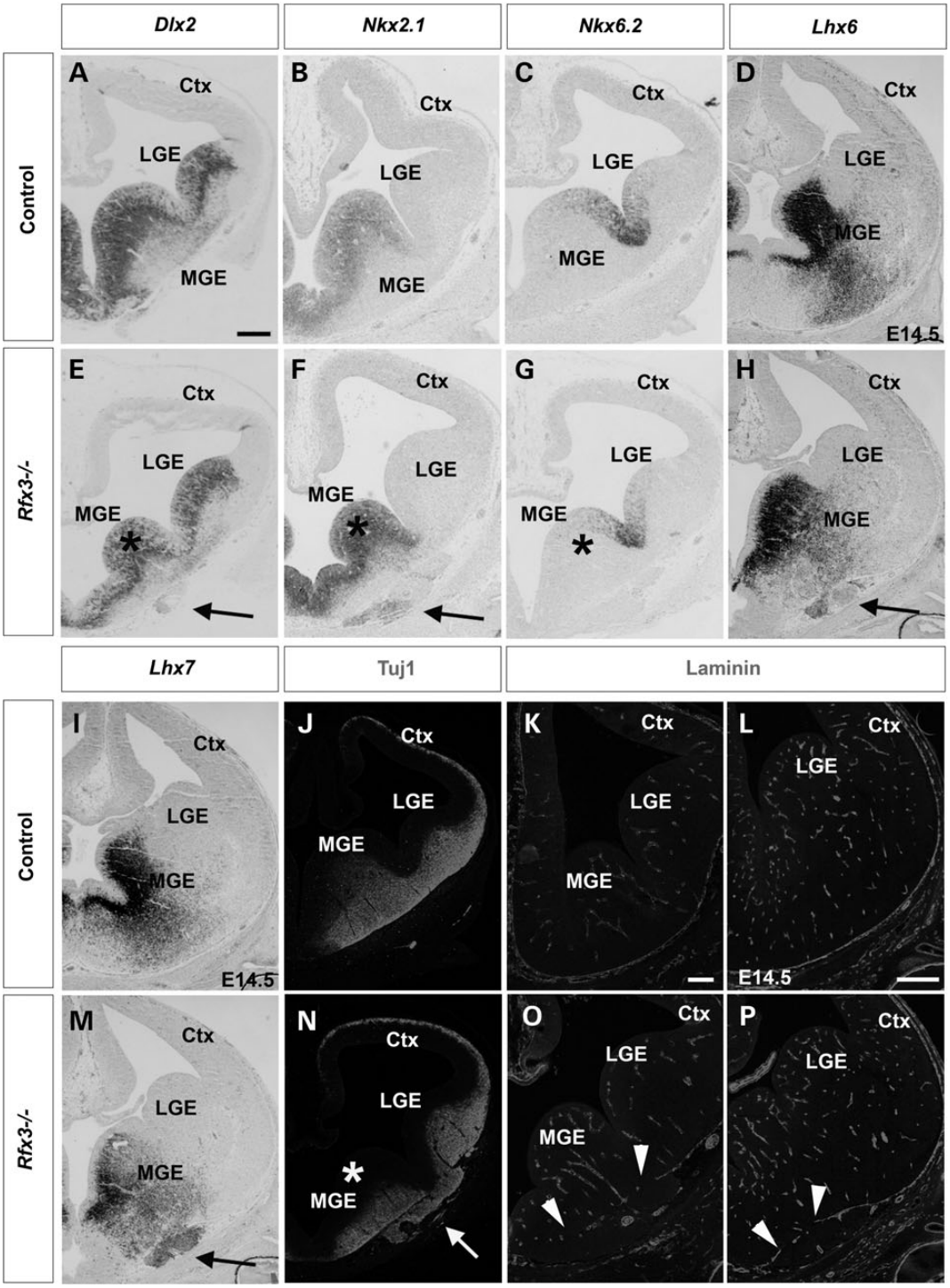

Figure 4. Patterning defects in the VT of *Rfx3*$^{-/-}$ mutant embryos. *In situ* hybridizations (**A–I** and **M**) and immunostainings (**J–L** and **N–P**) on E12.5 (A–C, E–G, J, K, N and O) and E14.5 (D, H, I, M, L and P) coronal sections with the indicated antibodies and probes, respectively. (A) *Dlx2* is expressed in the VT, including LGE and MGE, and also defines the PSPB. (B) *Nkx2.1* is specifically expressed in the MGE. (C) *Nkx6.2* expression defines the sulcus between the LGE and MGE. (E and F) The expression patterns of *Dlx2* and *Nkx2.1* are not changed in *Rfx3*$^{-/-}$ mutants, but *Dlx2*- and *Nkx2.1*-expressing cells ectopically accumulate outside the MGE mantle (arrows). (G) *Nkx6.2* expression is reduced in the *Rfx3*$^{-/-}$ VT. (D and I) *Lhx6* and *Lhx7* are strongly expressed within the MGE mantle. (H and M) In *Rfx3*$^{-/-}$ mutants, ectopic *Lhx6* and *Lhx7* expression is found in the heterotopias (arrows in H and M). (J) Tuj1staining labels the mantle of MGE, LGE and the cortical preplate. (N) *Rfx3*$^{-/-}$ embryos show a thinner MGE mantle (asterisk) and an ectopic accumulation of Tuj1^{+} cells outside the MGE mantle (arrow). (K and L) In control brains, laminin labels the basal lamina surrounding the VT. (O and P) In *Rfx3*$^{-/-}$ mutant brains, the basal lamina is abnormally disrupted (arrowheads). Scale bars: 100 µm.

expressed in ventral telencephalic progenitor cells, and *Netrin1* transcripts were also found in the MGE mantle (Fig. 7K and L). These expression patterns remain unaltered in *Rfx3*$^{-/-}$ embryos, but both genes are ectopically expressed in cells located in the heterotopias (Fig. 7O and P). Taken together, these expression analyses did not reveal changes in the overall *Sema5b*, *Sema6a*

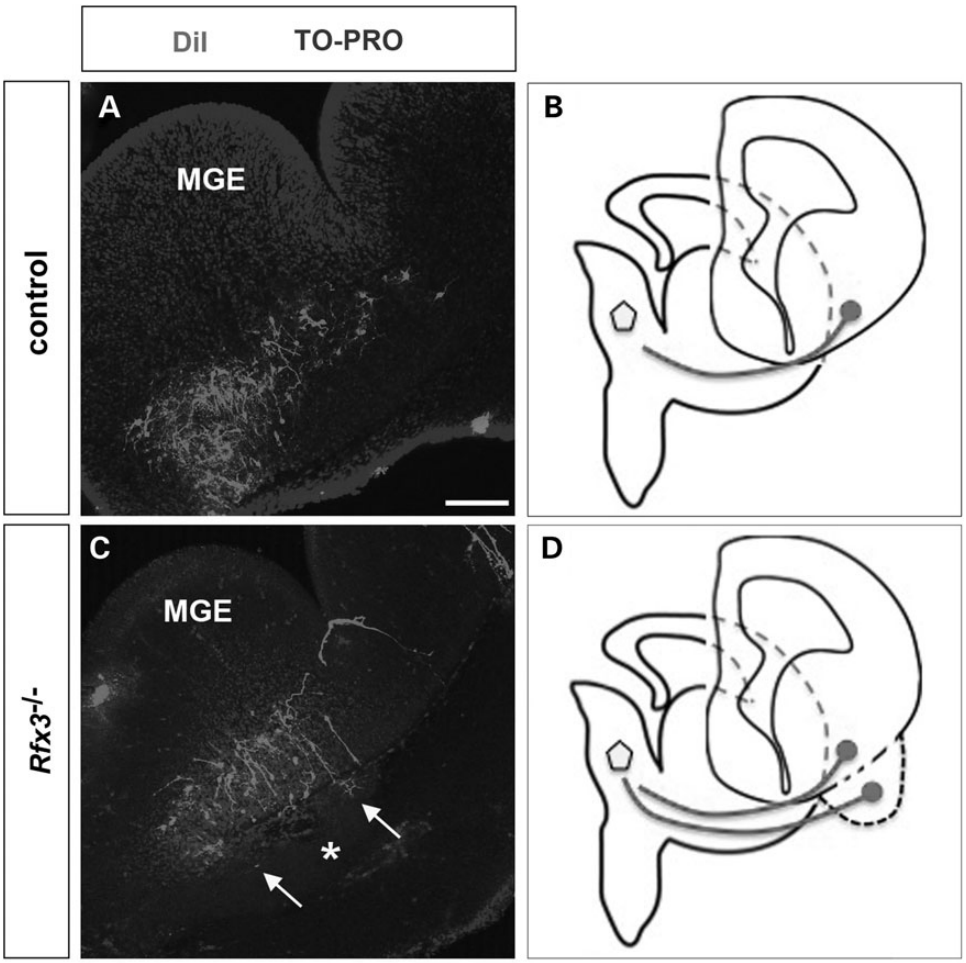

Figure 5. Abnormal formation of MGE pioneer neurons in *Rfx3*$^{-/-}$ mutants. (**A**) DiI placements into the E12.5 thalamus of control embryos retrogradely labeled cell bodies located in the MGE and their axons. (**C**) DiI placed in the E12.5 *Rfx3*$^{-/-}$ thalamus revealed pioneer neuron cell bodies and axons in the MGE mantle and in ectopic locations in the heterotopias (arrows in C label the cell bodies and the asterisk the heterotopia). (**B** and **D**) Schematic representation of a series of coronal sections showing the location and axonal projections of MGE pioneer neurons. Note that these neurons reside in the rostral MGE and project their axons caudally toward the diencephalon. Scale bar: 200 μm.

and *PlexinA4* expression patterns, but show differences in the organization of TCAs with respect to the expression domains of these guidance molecules and also indicate ectopic expression of axon guidance factors in the heterotopias.

The *Inpp5e* ciliary mouse mutant phenocopies the TCA pathfinding defects of *Rfx3*$^{-/-}$ mutants

The Rfx3 transcription factor has a prominent role in ciliogenesis by regulating the expression of many genes involved in cilia assembly and function, suggesting that the thalamocortical abnormalities of *Rfx3*$^{-/-}$ embryos are likely caused by structural and/or functional ciliary defects. However, scanning electron microscopy revealed that cilia are present in the diencephalon and telencephalon of E10.5 *Rfx3*$^{-/-}$ embryos without obvious morphological abnormalities (Supplementary Material, Fig. S6 and data not shown). To gain support for the involvement of cilia in the pathogenesis of these *Rfx3*$^{-/-}$ phenotypes, we characterized thalamocortical development in an additional ciliary mouse mutant that carries a mutation in the *Inpp5e* gene (29). *Inpp5e* encodes inositol polyphosphate-5-phosphatase E that hydrolyzes the 5-phosphate of the second messengers PI(4,5)P2 and PI (3,4,5)P3. The Inpp5e protein is localized at the axoneme of the primary cilium and has a role in cilia-mediated signaling and in regulating cilia stability (29,30). Moreover, its human homolog *INPP5E* is mutated in MORM and in Joubert syndrome (29,30). *Inpp5e* mouse mutants show defects in limb and kidney development typical for cilia dysfunction (29), but thalamocortical development has not been investigated yet. Similar to *Rfx3*$^{-/-}$ embryos, labeling of the thalamocortical tract in E18.5 *Inpp5e*$^{-/-}$ embryos by inserting DiI crystals into the thalamus revealed an abnormal broad trajectory of TCAs into the rostral cortex and a ventral deflection of TCAs toward the amygdala (Fig. 8A, B, E and F). This phenotype was confirmed by NF immunohistochemistry staining, which also showed the absence of heterotopias in the VT of *Inpp5e*$^{-/-}$ embryos (Fig. 8C, D, G and H). Next, we investigated the origin of this axonal phenotype. In the diencephalon of *Inpp5e* mutant embryos, *Shh* expression in the zli was more diffuse, and the *Gli1* expression domain is broader but thalamic patterning and neuronal specification were not obviously affected (Supplementary Material, Fig. S7). Similarly, a slight expansion in *Gli1* and *Ptc1* expression in the MGE had no obvious effect on dorsal/ventral patterning of the telencephalon (Supplementary Material, Fig. S8). Cortical lamination and the expression of

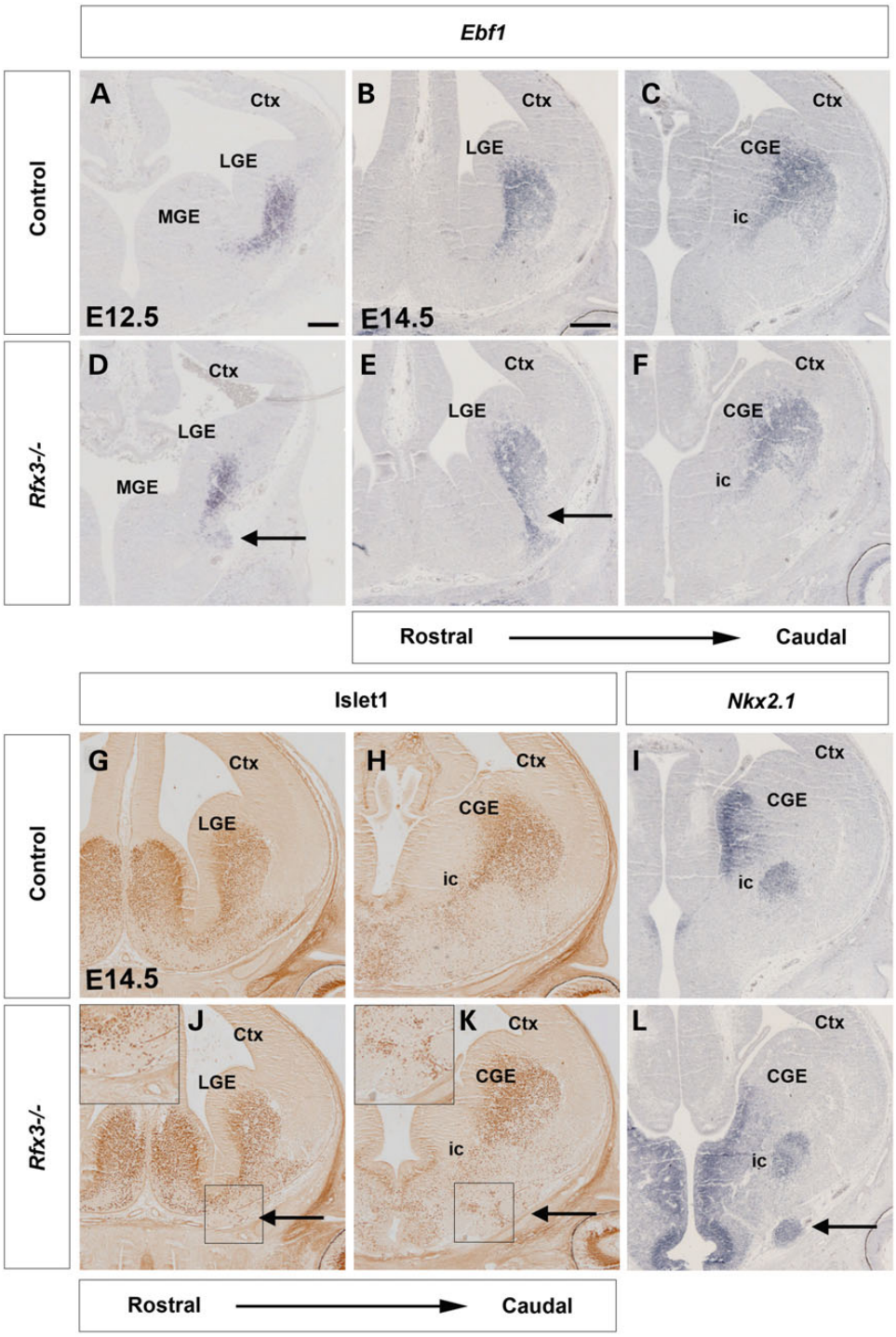

Figure 6. Formation of the ventral telencephalic corridor in *Rfx3*$^{-/-}$ mutants. Coronal sections through the brain of control (**A–C** and **G–I**) and *Rfx3*$^{-/-}$ mutant embryos (**D–F** and **J–L**) hybridized with the indicated probes or immunostained with the indicated antibodies. (A–F) *Ebf1* expression marks the corridor cells in E12.5 (A and D) and E14.5 (B, C, E and F) control and *Rfx3*$^{-/-}$ mutant embryos. (D–F) *Ebf1*$^{+}$ cells are misdirected toward the heterotopias in *Rfx3*$^{-/-}$ mutant sections (arrows in D and E). (G, H, J and K) Isl1/2 immunohistochemistry reveals the distribution of corridor cells in E14.5 control and mutant embryos. (J and K) In *Rfx3*$^{-/-}$ embryos, some Isl1/2^{+} cells are ectopically located in the heterotopias (insets and arrows). (I and L) *Nkx2.1* expression labels the ventricular zone and mantle of the MGE, whereas the ic remains *Nkx2.1* negative. (L) In the *Rfx3*$^{-/-}$ MGE, some *Nkx2.1* expressing cells are ectopically located in the heterotopias (arrow). Scale bar: 100 µm.

Tbr1 and Ctip2 characteristic of corticofugal projection neurons also appeared normal in *Inpp5e*$^{-/-}$ embryos (Supplementary Material, Fig. S9). In contrast, the MGE corridor was broader and the groups of *Sema6a*- and *PlexinA4*-expressing cells delineating the corridor were not discernible in mutant embryos (Supplementary Material, Figs S10 and S11), suggesting that defective ventral telencephalic development underlies the TCA pathfinding defects. Moreover, the similar ventral deflection of TCAs in *Rfx3*$^{-/-}$ and *Inpp5e*$^{-/-}$ embryos strongly implicates cilia dysfunction as the major cause of this phenotype in *Rfx3*$^{-/-}$ mutants.

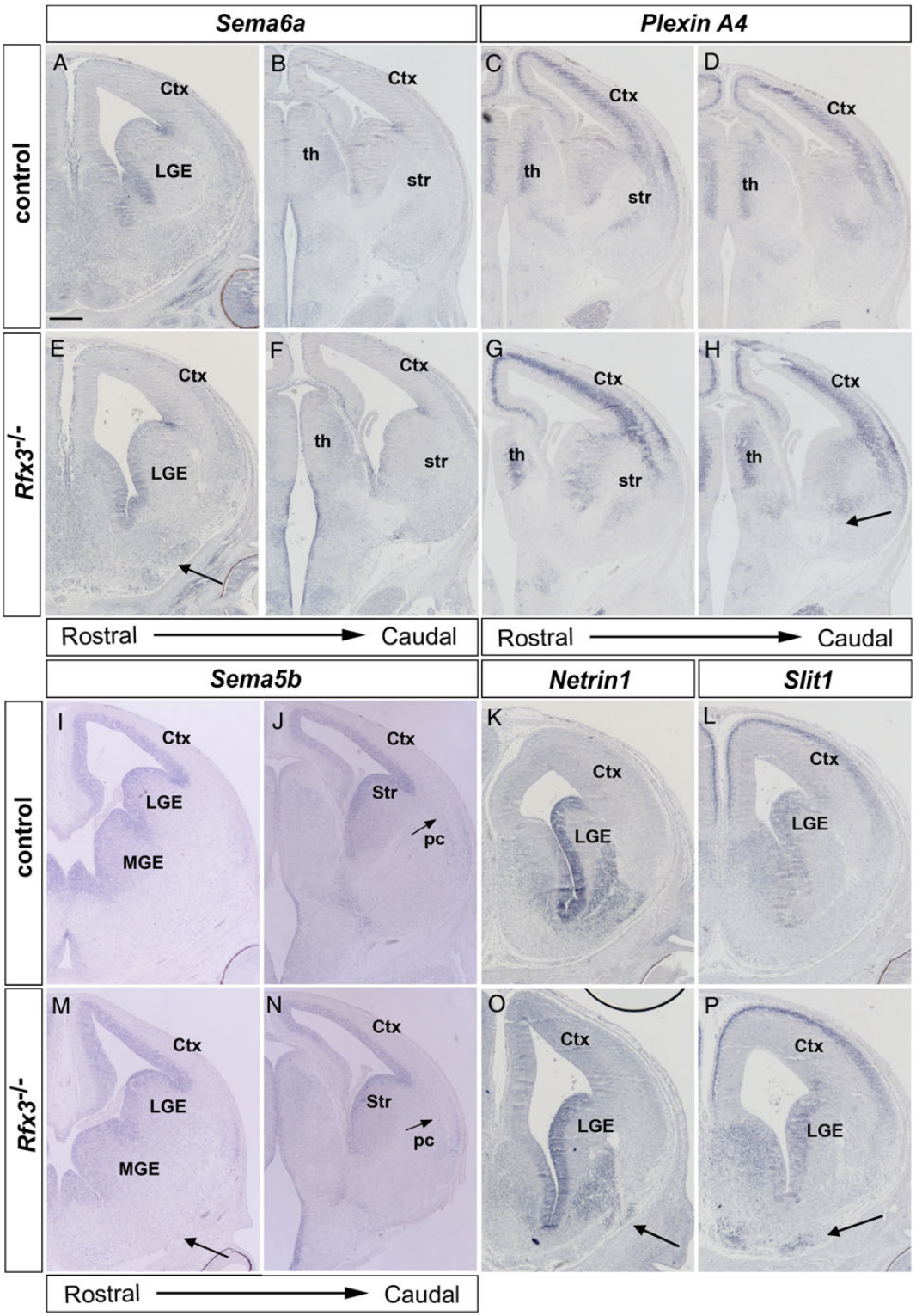

Figure 7. The *Rfx3*$^{-/-}$ heterotopias express thalamocortical guidance molecules. Coronal sections through the brain of control (**A–D**, **I–L**) and *Rfx3*$^{-/-}$ mutants (**E–H**, **M–P**) hybridized with the indicated probes. (A, B, E and F) At rostral levels, *Sema6a* shows expression in the ventral telencephalic ventricular zone and weak expression in the heterotopia of *Rfx3*$^{-/-}$ embryos (arrow). Caudally, *Sema6a* is expressed along the path of TCAs in the prethalamus and VT, and its expression is not affected in *Rfx3*$^{-/-}$ mutants. (C) *PlexinA4* is expressed in the thalamus and delineates the corridor ventrally and dorsally (arrows). (D) *PlexinA4*-expressing cells also reside in the caudal VT where TCAs normally not project. (G and H) In *Rfx3*$^{-/-}$ embryos, *PlexinA4* expression is largely maintained in the VT and thalamus; however, in the caudal VT, it is expressed adjacent to an ectopic axon bundle projecting toward the amygdala (arrow). (I, J, M and N) *Sema5b* expression in telencephalic progenitors and in neurons of the piriform cortex (pc) is maintained in *Rfx3*$^{-/-}$ embryos. (K, L, O and P) *Netrin1* and *Slit1* are expressed in ventral telencephalic progenitor cells, and *Netrin1* transcripts were also found in the MGE mantle in both control and *Rfx3*$^{-/-}$ embryos, but both genes are ectopically expressed in the heterotopias (arrows in O and P). Scale bar: 100 µm.

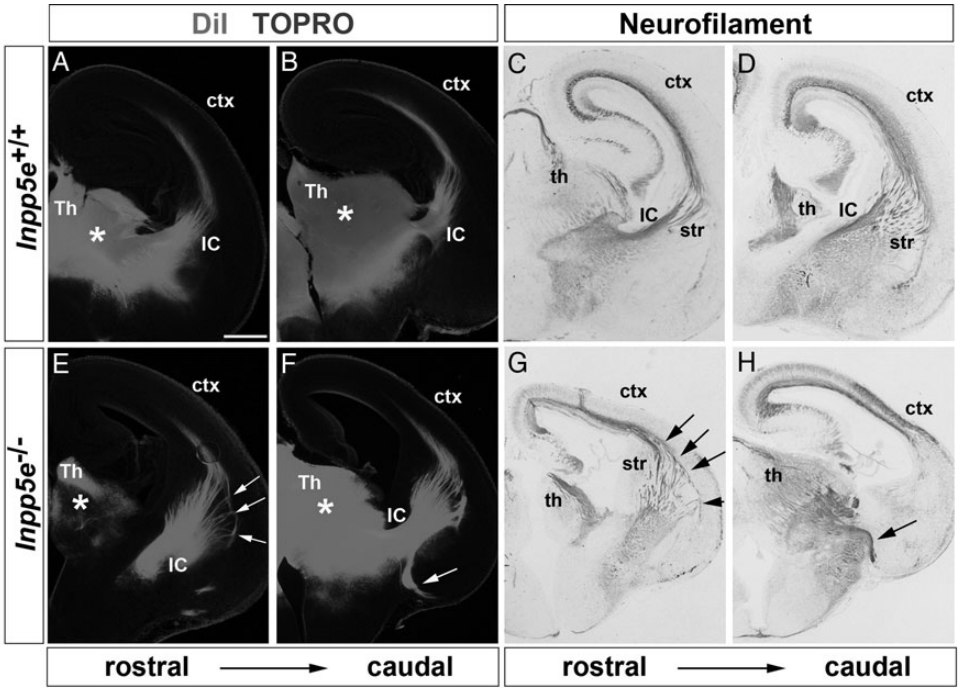

Figure 8. TCA pathfinding defects in E18.5 *Inpp5e*$^{-/-}$ brains. Coronal sections through the brains of control (**A–D**) and *Inpp5e*$^{-/-}$ (**E–H**) embryos. (A, B, E and F) DiI placements in the thalamus (asterisks) revealed the TCA trajectory in control embryos. (A and B) In *Inpp5e*$^{-/-}$ mutants, TCAs cross the PSPB in a broad area (arrows in E) and some TCAs form an ectopic axon bundle running ventrally toward the pial surface (arrow in F). (C, D, G and H) NF immunostainings showed a broadened entry area of TCAs into the cortex (arrows in G) and an ectopic axon bundle running ventrally toward the amygdala in *Inpp5e*$^{-/-}$ embryos (arrow in H). Scale bar: 100 µm.

The Gli3 repressor does not rescue TCA pathfinding and heterotopia formation in *Rfx3*$^{-/-}$ mutants

Finally, we addressed the cilia-regulated signaling pathway(s) which could underlie the TCA and heterotopia phenotype in *Rfx3* mutants. During forebrain development, primary cilia are essential for the processing of the Gli3 protein thereby controlling the balance between Gli3 repressor (Gli3R) and activator forms (Gli3A). Recently, we showed that this balance is disturbed in the *Rfx3*$^{-/-}$ forebrain (16). *Rfx3* mutants also phenocopy the thalamocortical abnormalities of the *Gli3* hypomorphic mutant *Gli3*^{Pdn} (10). In addition, the olfactory bulb phenotype of the *Ftm* cilia mutant is rescued in *Ftm*$^{-/-}$;*Gli3*$^{\triangle 699/+}$ embryos (31) in which the *Gli3*$^{\triangle 699}$ allele exclusively produces a short Gli3 isoform that resembles Gli3R (32) in a cilia-independent manner. These findings raised the possibility that the TCA pathfinding defects in *Rfx3*$^{-/-}$ embryos are caused by disrupting the Gli3R/Gli3A ratio, and we therefore analyzed thalamocortical tract and heterotopia formation in *Rfx3*$^{-/-}$;*Gli3*$^{\triangle 699/+}$ mutants. However, *Rfx3*$^{-/-}$;*Gli3*$^{\triangle 699/+}$ mutants still showed an abnormal projection of TCAs toward the amygdala and formed heterotopias in the ventrorostral telencephalon (Supplementary Material, Fig. S12). Therefore, re-introduction of Gli3R is not sufficient to rescue these defects unlike the previously described rescue of the Ftm olfactory bulb phenotype (31). This finding could be explained by a requirement for Gli activator and not Gli repressor function in VT patterning and indeed, Gli3 western blots showed that the levels of Gli3R are not altered in the VT of *Rfx3*$^{-/-}$ embryos (Supplementary Material, Fig. S13).

Discussion

Ciliopathies, syndromes caused by dysfunction of the primary cilium, are often associated with MR; however, the underlying pathogenesis remains largely unknown. Here, we investigated the development of the forebrain in mice mutant for the ciliogenic transcription factor Rfx3. We show that *Rfx3* mutants display the formation of heterotopias in the VT and patterning defects in the prethalamus. Moreover, the development of guidepost neurons, which are provided by the VT and which guide TCAs from the thalamus into the cortex, is affected. In fact, many TCAs are unable to leave the thalamus or mis-project toward the amygdala after entry into the VT. As a similar ventral deflection of TCAs into the VT is also found in *Inpp5e* mutants, these findings provide a novel role for primary cilia in the development of the thalamocortical tract.

Rfx3 is required for patterning the VT and the diencephalon

Recent analyses have shown a prominent role of primary cilia in forebrain development, but only few cilia mouse mutants with forebrain phenotypes have been described yet. These analyses were also limited by severe patterning defects (33,34) or did not analyze diencephalic development (31). Therefore, roles of primary cilia in the VT and in the diencephalon remain largely unknown or have not been analyzed at all. *Rfx3* mutant mice provide a useful tool for studying such functions. In contrast to previously analyzed cilia mutants, these animals show a relatively mild alteration in the Gli3 activator/Gli3 repressor ratio in the forebrain (16), an important determinant of Shh controlled patterning processes.

Interestingly, *Rfx3*$^{-/-}$ embryos show multiple and complex abnormalities in the VT. First, the size of the *Rfx3*$^{-/-}$ MGE mantle is reduced. Secondly, *Rfx3*$^{-/-}$ embryos form heterotopias in which the basal lamina is disrupted and telencephalic cells are located outside the mantle zone. These heterotopias are a complex mixture of different cell types including progenitor cells (*Dlx2*$^{+}$ and

Nkx2.1^{+}) and MGE- (*Lhx6*$^{+}$ and *Lhx7*$^{+}$) and LGE-(*Ebf1*$^{+}$ and Isl1/2^{+}) derived neurons. The heterotopias also express *Shh* (16) and several genes encoding axon guidance molecules (Fig. 7). The molecular mechanisms underlying their formation remain unknown, but could relate to altered Shh signaling which could lead to an early overproduction of MGE neurons. While qRT-PCR analysis using the whole VT revealed a mild up-regulation for *Ptc1* but not for *Gli1* expression, *in situ* hybridization indicated reduced expression of the Shh target genes *Ptc1*, *Gli1* and *Nkx6.2* in the ventricular zone of the VT. This discrepant finding could be attributed to the *Shh* expression in the heterotopias (16) and a concomitant up-regulation of Shh signaling in this ectopic tissue. Alternatively, the heterotopias could be formed by an over-migration of ventral telencephalic neurons (35), which could also contribute to the size reduction of the MGE mantle region, with neurons settling outside the MGE mantle.

The *Rfx3* mutation also affects the patterning of the prethalamus as indicated by an expansion of Nkx2.2 and Olig2 expression and a concomitant reduction of Pax6 expression. These alterations in marker gene expression are consistent with known roles of Shh signaling. Prethalamic Nkx2.2 expression is reduced in the diencephalon of mouse embryos in which Shh signaling is inhibited (25), whereas Nkx2.2 and Olig2 expression is expanded after increasing Shh signaling in the diencephalon (25,36). In addition, tissue transplant studies in chick embryos show that ectopic expression of Shh negatively controls diencephalic Pax6 expression (37). Similarly, the expression of the Shh target genes *Gli1* and *Ptc1* is expanded in the prethalamus; however, our qRT-PCR analysis could not detect significant changes in the expression levels of these markers in the diencephalon. Due to the comparatively small size of the prethalamic progenitor domain within the diencephalon, it is possible that changes in *Gli1* and *Ptc1* expression in the prethalamus are too small to be detected within the whole diencephalic tissue. Alternatively, alterations in other signaling pathways could be responsible for the prethalamic defects. Wnt/β-catenin plays well-characterized roles in establishing the zli (38) and in specifying progenitor identity in the thalamus (39), whereas Fgf signaling controls the development of GABAergic neurons in the prethalamus and rostral thalamus (40). However, roles for either pathway in prethalamic patterning have to be identified yet. In contrast, *Rfx3*$^{-/-}$ embryos showed no obvious defect in thalamic development. The specification of the thalamic nuclei appears to be delayed compared with the differentiation of prethalamic neurons and is concomitant with a down-regulation of Shh signaling, suggesting that molecules others than *Shh* play a more prominent role in specifying thalamic nuclei (41). Regardless of the exact mechanism, our data clearly indicate novel roles for primary cilia in the development of the VT and in the patterning of the prethalamus.

Corticothalamic/thalamocortical tract defects in *Rfx3*$^{-/-}$ mutants

Our analyses also revealed pathfinding defects of thalamocortical and CTAs in *Rfx3*$^{-/-}$ mutants occurring subsequently to patterning defects. Some thalamic axons reach the cortex whereas others are either not able to exit the dorsal thalamus, or after having entered the VT mis-project toward the amygdala. Since thalamic patterning, production of post-mitotic neurons and initial growth of TCAs are not obviously affected, cell-autonomous defects in thalamic neurons are unlikely to underlie these pathfinding defects, but this requires further testing in transplantation experiments. In contrast, development of the prethalamus and the VT is compromised in *Rfx3*$^{-/-}$ mutants. Both structures give rise to multiple neuronal cell types playing important roles in the guidance of thalamocortical/CTAs (17). Indeed, we show here an abnormal migration of corridor cells and MGE pioneer neurons into the ventral telencephalic heterotopias of *Rfx3*$^{-/-}$ mutants. Similarly, mis-patterning of the prethalamus might have affected the development of prethalamic pioneer neurons, which normally project their axons into the thalamus thereby providing a scaffold for TCAs. Given the importance of pioneer neurons in the development of forebrain connections (10,42–46), defects in the prethalamic pioneer neurons might be responsible for the clustering of TCAs in the diencephalon; however, we currently lack the molecular markers to test this hypothesis.

Moreover, our analysis provides first insights into the cellular and molecular mechanisms by which *Rfx3* controls thalamocortical tract formation. The Rfx transcription factors regulate the transcription of genes important for ciliogenesis and function, suggesting that ciliary defects may underlie the abnormal TCA pathfinding in *Rfx3*$^{-/-}$ embryos. While cilia are present without obvious morphological abnormalities in the *Rfx3* mutant forebrain, their function might be affected as in *Ift88* hypomorphic mutants which have severe telencephalic patterning defects (34). Taken together with our finding that inactivating two genes with essential but different roles in cilia, namely *Rfx3* or *Inpp5e*, which encode a transcription factor controlling cilia assembly or an enzyme regulating cilia signaling and stability, respectively, result in an highly similar TCA phenotype suggests that cilia dysfunction underlies this TCA pathfinding defect. The ectopic projection of TCAs toward the amygdala in *Rfx3*$^{-/-}$ and *Inpp5e*$^{-/-}$ embryos also phenocopies the TCA pathfinding errors in the *Gli3* hypomorphic mutant *Gli3*$^{Pdn/Pdn}$ (10), suggesting altered Gli3 processing as the key cilia controlled pathway responsible for this phenotype. However, while the Gli3R/Gli3FL ratio is altered in the whole forebrain (16), Gli3 western blotting did not reveal significant changes in this ratio in the VT of *Rfx3*$^{-/-}$ embryos, similar to our previous finding in *Gli3*$^{Pdn/Pdn}$ mutants (10). Moreover, re-introducing a Gli3R allele in an *Rfx3*$^{-/-}$ mutant background does not ameliorate the TCA abnormalities, unlike the rescue of olfactory bulb formation in *Ftm*$^{-/-}$ embryos (31) or of the callosal defects in *Rfx3*$^{-/-}$ embryos (B. Durand, manuscript submitted). These findings rule out the involvement of altered Gli3 to Gli3R processing. Alternatively, these data suggest that there could be different requirements for *Gli3* repressor and activator functions in the dorsal telencephalon and VT. It will therefore be interesting to aim at rescuing the *Rfx3* phenotype using a *Gli3* mutant that predominantly forms Gli3A (47).

Finally, the formation of neural heteropias might also affect CTA pathfinding in the VT. The ventral TCA deflection and heterotopia formation occur at different rostro/caudal levels. In contrast, CTAs are deflected at rostral levels where heterotopias are present, and this deflection is absent in *Inpp5e*$^{-/-}$ and *Gli3*$^{Pdn/Pdn}$ embryos which lack heterotopias. Moreover, the heterotopias contain Ebf1^{+} and Isl1/2^{+} neurons. These cells normally migrate from the LGE in the MGE to form a corridor permissive for TCAs and CTAs, but are abnormally scattered throughout the MGE mantle and even form a stream of cells connecting the LGE with the heterotopias. These also contain cells expressing *Netrin1* and *Slit1*, which individually act as chemoattractant or repellent of TCAs, respectively, but their combined action is required for the rostral/caudal sorting of TCAs (12). Therefore, the heterotopias could provide alternative migration routes for CTAs toward the thalamus (27).

Conclusion

Our study highlights essential roles of *Rfx3* for the correct development of the VT and the prethalamus and emphasizes how subtle defects in these tissues can lead to severe pathfinding defects in the thalamocortical tract. These findings are highly relevant to human ciliopathies, which are often associated with MR. The thalamocortical tract as a major forebrain axon tract conveys most of the sensory information from the environment to the cerebral cortex and its disruption is predicted to interfere with the normal functioning of the cortex. Indeed, development of the thalamus and cortex is tightly linked and abnormalities in the thalamocortical pathways correlate with sensory and motor deficits in preterm born children (48,49). In addition, Bardet-Biedl syndrome patients have recently been reported with a reduced thalamic size (50,51). Moreover, we show here that an identical TCA pathfinding defect is present in mice mutant for the *Inpp5e* gene, whose human homolog is mutated in Joubert Syndrome (29,30). It will therefore be interesting to analyze thalamocortical tract formation in ciliopathy patients which could lead to a new understanding of the pathogenesis of MR in these patients.

Materials and Methods

Mice

All animal research has been conducted according to relevant national and international guidelines. *Rfx3*-deficient embryos were generated and genotyped as previously described (14). *Gli3*$^{\triangle 699}$ and *Inpp5e* null mutant mice used in this work have previously been described (29,32). For each marker and each stage, 3–6 mutant embryos were analyzed and compared with 3–6 controls. All reported phenotypes were fully penetrant.

In situ hybridization and immunohistochemistry

Antisense RNA probes for *Dbx1* (52); *Dlx2* (53); *Ebf1* (11); *Gbx2* (54); *Gli1* (55); *Ngn2* (56); *Nkx2.1* (57); *Lhx2* (EST2101448); *Lhx6* and *Lhx7* (58); *Nkx6.2* (59); *Ptc* (60) and *Shh* (61) were labeled with digoxigenin. *In situ* hybridization on 10 µm serial paraffin sections of mouse brains was performed as described (62).

Immunohistochemical analysis was performed as described previously (62) using antibodies against the following molecules: β-III-tubulin (Tuj1 antibody; 1 : 1000, Sigma); CR (1 : 1000, CHEMICON); Gsh2 (1 : 2500, a gift from K. Campbell, Cincinnati Children's Hospital Medical Center, OH); Isl1/2 (1 : 100; DSHB); laminin (1 : 100, Sigma); NF (1 : 5; DSHB); Nkx2.2 (1 : 50, DSHB); Olig2 (1 : 1000, Millipore) and Pax6 (1 : 200; DSHB). Primary antibodies for immunohistochemistry were detected with Alexa- or Cy2/3-conjugated fluorescent secondary antibodies, and sections were incubated the nuclear counterstain TOPRO3 (0.2 µM) for 3 min after secondary antibody application. For non-fluorescent detection, we used biotinylated goat anti-mouse/rabbit antibodies (Dako) followed by avidin-HRP and DAB detection (Vector Laboratories).

Carbocyanine dye placements and analysis

Brains were isolated and fixed overnight in 4% (w/v) paraformaldehyde (PFA) at 4°C. For thalamic placements, caudal parts of the brains were removed with a coronal cut to expose the caudal surface of the dorsal thalamus. Depending on brain size, single crystals were placed at one to three positions along the dorsoventral extent of the dorsal thalamus. For cortical labelings, DiI was directly placed on the cortical surface. For each axon tract and for each stage, at least three control and three *Rfx3*$^{-/-}$ embryos were used. Dyes were allowed to diffuse at room temperature for 4–8 weeks in 4% (w/v) PFA in PBS. Brains were rinsed in PBS, embedded in 4% agarose and sectioned coronally on a vibratome at 100–120 µm. Sections were cleared in 9 : 1 glycerol : PBS solution containing the nuclear counterstain TOPRO3 (0.2 µM) overnight at 4°C.

Scanning electron microscopy

E10.5 embryos were dissected in PBS at 400 mOsm. Brains were removed, cut into small fragments and fixed overnight at 4°C in PBS (200 mOsm)/2% glutaraldehyde. Brain samples were then washed several times in PBS (400 mOsm) and postfixed for 15 min in PBS (400 mOsm)/1% OsO_4 (Euromedex, France). Fixed brain samples were washed extensively with distilled water and dehydrated in a graded series of ethanol solutions and finally in acetone. Brain samples were then prepared for scanning electron microscopy by the critical point freeze–dry procedure (Balzers-Union, CPD020). Samples were surface-coated using a gold/palladium spattering device (Hummer 2, Technics) under optimal conditions for 1 min 30 s, and observed with a scanning electron microscope (S800, Phillips) at 15 keV. Observations were performed at the Centre for Microstructure Analysis of the University of Lyon.

Quantitative RT-PCR

Total RNA was extracted from the dorsal telencephalon, the VT and the diencephalon of six wild-type and six *Rfx3*$^{-/-}$ E12.5 embryos using the Nucleospin RNA XS kit (Macherey Nagel). cDNAs were synthesized using 0.8 µg of total RNA, 200 ng of random primers (Promega) and 200 units of RevertAid H Minus M-MuLV Reverse Transcriptase (Fermentas) according to the manufacturer's instructions in a final volume of 20 µl. Real-time PCR was performed as previously described (63) on 2 µl of cDNA diluted one-fifth using the SYBR Green fluorescent mix (Roche) in a LC480 LightCycler (Roche). Primer sequences are available upon request. According to melting point analysis, only one PCR product was amplified. RNA extracted from heterozygous samples was used to generate a standard quantification curve for each gene, allowing the calculation of relative amounts of transcripts in the samples. The expression of each gene was normalized using the housekeeping gene *Tbp*. Statistical analysis was performed with the non-parametric Mann–Whitney test using the GraphPad Prism software.

Western blotting

Protein was extracted from the VT of E13.5 wild-type and *Rfx3*$^{-/-}$ embryos as described previously (10). About 10 µg protein were subjected to gel electrophoresis on a 3–8% gradient Tris-acetate gel (Invitrogen), and protein was transferred to a nitrocellulose membrane, which was incubated with rabbit polyclonal anti-Gli3 antibody (1 : 500; Abcam). After incubating with a horseradish peroxidase-conjugated anti-rabbit IgG secondary antibody (1 : 2000; Dako), signal was detected using an ECL Plus detection kit (Amersham GE healthcare). Band intensity was determined using the ImageJ software. The levels of Gli3R, Gli3A and the Gli3R/Gli3A ratio were compared between wild-type and mutant tissue using the Mann–Whitney test.

Supplementary Material

Supplementary Material is available at *HMG* online.

Acknowledgements

We thank Drs David J. Price, John Mason and Tom Pratt for critical comments on the manuscript and Isabel Martin Caballero and Kevin Adutwum-Ofosu for extremely helpful discussions. We are grateful to Trudi Gillespie for help with confocal imaging, Elodie Vallin for animal husbandry, Carine Benadiba for performing scanning EM on embryos and Charline Maire for help with quantitative RT-PCR.

Conflict of Interest statement. None declared.

Funding

This work was supported by grants from the Medical Research Council (T.T.). Work in the Durand Laboratory was supported by the Fondation pour la Recherche Medicale (FRM, Equipe DEQ20090515392 and DEQ2013029168) and the Agence Nationale de la Recherche (ANR).

References

1. Goetz, S.C. and Anderson, K.V. (2010) The primary cilium: a signalling centre during vertebrate development. *Nat. Rev. Genet.*, **11**, 331–344.
2. Badano, J.L., Mitsuma, N., Beales, P.L. and Katsanis, N. (2006) The ciliopathies: an emerging class of human genetic disorders. *Annu. Rev. Genomics Hum. Genet.*, **7**, 125–148.
3. Tobin, J.L. and Beales, P.L. (2009) The nonmotile ciliopathies. *Genet. Med.*, **11**, 386–402.
4. Guemez-Gamboa, A., Coufal, N.G. and Gleeson, J.G. (2014) Primary cilia in the developing and mature brain. *Neuron*, **82**, 511–521.
5. Valente, E.M., Rosti, R.O., Gibbs, E. and Gleeson, J.G. (2014) Primary cilia in neurodevelopmental disorders. *Nat. Rev. Neurol.*, **10**, 27–36.
6. Grant, E., Hoerder-Suabedissen, A. and Molnar, Z. (2012) Development of the corticothalamic projections. *Front. Neurosci.*, **6**, 53.
7. Metin, C. and Godement, P. (1996) The ganglionic eminence may be an intermediate target for corticofugal and thalamocortical axons. *J. Neurosci.*, **16**, 3219–3235.
8. Molnar, Z., Adams, R. and Blakemore, C. (1998) Mechanisms underlying the early establishment of thalamocortical connections in the rat. *J. Neurosci.*, **18**, 5723–5745.
9. Tuttle, R., Nakagawa, Y., Johnson, J.E. and O'Leary, D.D. (1999) Defects in thalamocortical axon pathfinding correlate with altered cell domains in Mash-1-deficient mice. *Development*, **126**, 1903–1916.
10. Magnani, D., Hasenpusch-Theil, K., Jacobs, E.C., Campagnoni, A.T., Price, D.J. and Theil, T. (2010) The Gli3 hypomorphic mutation Pdn causes selective impairment in the growth, patterning, and axon guidance capability of the lateral ganglionic eminence. *J. Neurosci.*, **30**, 13883–13894.
11. Lopez-Bendito, G., Cautinat, A., Sanchez, J.A., Bielle, F., Flames, N., Garratt, A.N., Talmage, D.A., Role, L.W., Charnay, P., Marin, O. *et al.* (2006) Tangential neuronal migration controls axon guidance: a role for neuregulin-1 in thalamocortical axon navigation. *Cell*, **125**, 127–142.
12. Bielle, F., Marcos-Mondejar, P., Leyva-Diaz, E., Lokmane, L., Mire, E., Mailhes, C., Keita, M., Garcia, N., Tessier-Lavigne, M., Garel, S. *et al.* (2011) Emergent growth cone responses to combinations of Slit1 and Netrin 1 in thalamocortical axon topography. *Curr. Biol.*, **21**, 1748–1755.
13. Baas, D., Meiniel, A., Benadiba, C., Bonnafe, E., Meiniel, O., Reith, W. and Durand, B. (2006) A deficiency in RFX3 causes hydrocephalus associated with abnormal differentiation of ependymal cells. *Eur. J. Neurosci.*, **24**, 1020–1030.
14. Bonnafe, E., Touka, M., AitLounis, A., Baas, D., Barras, E., Ucla, C., Moreau, A., Flamant, F., Dubruille, R., Couble, P. *et al.* (2004) The transcription factor RFX3 directs nodal cilium development and left-right asymmetry specification. *Mol. Cell. Biol.*, **24**, 4417–4427.
15. Thomas, J., Morle, L., Soulavie, F., Laurencon, A., Sagnol, S. and Durand, B. (2010) Transcriptional control of genes involved in ciliogenesis: a first step in making cilia. *Biol. Cell.*, **102**, 499–513.
16. Benadiba, C., Magnani, D., Niquille, M., Morle, L., Valloton, D., Nawabi, H., Ait-Lounis, A., Otsmane, B., Reith, W., Theil, T. *et al.* (2012) The ciliogenic transcription factor RFX3 regulates early midline distribution of guidepost neurons required for corpus callosum development. *PLoS Genet.*, **8**, e1002606.
17. Molnar, Z., Garel, S., Lopez-Bendito, G., Maness, P. and Price, D.J. (2012) Mechanisms controlling the guidance of thalamocortical axons through the embryonic forebrain. *Eur. J. Neurosci.*, **35**, 1573–1585.
18. Chen, L., Guo, Q. and Li, J.Y. (2009) Transcription factor Gbx2 acts cell-nonautonomously to regulate the formation of lineage-restriction boundaries of the thalamus. *Development*, **136**, 1317–1326.
19. Hevner, R.F., Miyashita-Lin, E. and Rubenstein, J.L. (2002) Cortical and thalamic axon pathfinding defects in Tbr1, Gbx2, and Pax6 mutant mice: evidence that cortical and thalamic axons interact and guide each other. *J. Comp. Neurol.*, **447**, 8–17.
20. Miyashita-Lin, E.M., Hevner, R., Wassarman, K.M., Martinez, S. and Rubenstein, J.L. (1999) Early neocortical regionalization in the absence of thalamic innervation. *Science*, **285**, 906–909.
21. Lopez-Bendito, G., Flames, N., Ma, L., Fouquet, C., Di Meglio, T., Chedotal, A., Tessier-Lavigne, M. and Marin, O. (2007) Robo1 and Robo2 cooperate to control the guidance of major axonal tracts in the mammalian forebrain. *J. Neurosci.*, **27**, 3395–3407.
22. Puelles, L. and Rubenstein, J.L. (1993) Expression patterns of homeobox and other putative regulatory genes in the embryonic mouse forebrain suggest a neuromeric organization. *Trends Neurosci.*, **16**, 472–479.
23. Shimamura, K., Hartigan, D.J., Martinez, S., Puelles, L. and Rubenstein, J.L. (1995) Longitudinal organization of the anterior neural plate and neural tube. *Development*, **121**, 3923–3933.
24. Vue, T.Y., Aaker, J., Taniguchi, A., Kazemzadeh, C., Skidmore, J.M., Martin, D.M., Martin, J.F., Treier, M. and Nakagawa, Y. (2007) Characterization of progenitor domains in the developing mouse thalamus. *J. Comp. Neurol.*, **505**, 73–91.
25. Vue, T.Y., Bluske, K., Alishahi, A., Yang, L.L., Koyano-Nakagawa, N., Novitch, B. and Nakagawa, Y. (2009) Sonic hedgehog signaling controls thalamic progenitor identity and nuclei specification in mice. *J. Neurosci.*, **29**, 4484–4497.
26. Flandin, P., Zhao, Y., Vogt, D., Jeong, J., Long, J., Potter, G., Westphal, H. and Rubenstein, J.L. (2011) Lhx6 and Lhx8 coordinately induce neuronal expression of Shh that controls the generation of interneuron progenitors. *Neuron*, **70**, 939–950.
27. Little, G.E., Lopez-Bendito, G., Runker, A.E., Garcia, N., Pinon, M.C., Chedotal, A., Molnar, Z. and Mitchell, K.J. (2009) Specificity and plasticity of thalamocortical connections in Sema6A mutant mice. *PLoS Biol.*, **7**, e98.
28. Bielle, F., Marcos-Mondejar, P., Keita, M., Mailhes, C., Verney, C., Nguyen Ba-Charvet, K., Tessier-Lavigne, M., Lopez-

Bendito, G. and Garel, S. (2011) Slit2 activity in the migration of guidepost neurons shapes thalamic projections during development and evolution. *Neuron*, **69**, 1085–1098.
29. Jacoby, M., Cox, J.J., Gayral, S., Hampshire, D.J., Ayub, M., Blockmans, M., Pernot, E., Kisseleva, M.V., Compere, P., Schiffmann, S.N. *et al.* (2009) INPP5E mutations cause primary cilium signaling defects, ciliary instability and ciliopathies in human and mouse. *Nat. Genet.*, **41**, 1027–1031.
30. Bielas, S.L., Silhavy, J.L., Brancati, F., Kisseleva, M.V., Al-Gazali, L., Sztriha, L., Bayoumi, R.A., Zaki, M.S., Abdel-Aleem, A., Rosti, R.O. *et al.* (2009) Mutations in INPP5E, encoding inositol polyphosphate-5-phosphatase E, link phosphatidyl inositol signaling to the ciliopathies. *Nat. Genet.*, **41**, 1032–1036.
31. Besse, L., Neti, M., Anselme, I., Gerhardt, C., Ruther, U., Laclef, C. and Schneider-Maunoury, S. (2011) Primary cilia control telencephalic patterning and morphogenesis via Gli3 proteolytic processing. *Development*, **138**, 2079–2088.
32. Böse, J., Grotewold, L. and Rüther, U. (2002) Pallister-Hall syndrome phenotype in mice mutant for Gli3. *Hum. Mol. Genet.*, **11**, 1129–1135.
33. Stottmann, R.W., Tran, P.V., Turbe-Doan, A. and Beier, D.R. (2009) Ttc21b is required to restrict sonic hedgehog activity in the developing mouse forebrain. *Dev. Biol.*, **335**, 166–178.
34. Willaredt, M.A., Hasenpusch-Theil, K., Gardner, H.A., Kitanovic, I., Hirschfeld-Warneken, V.C., Gojak, C.P., Gorgas, K., Bradford, C.L., Spatz, J., Wolfl, S. *et al.* (2008) A crucial role for primary cilia in cortical morphogenesis. *J. Neurosci.*, **28**, 12887–12900.
35. Cappello, S., Bohringer, C.R., Bergami, M., Conzelmann, K.K., Ghanem, A., Tomassy, G.S., Arlotta, P., Mainardi, M., Allegra, M., Caleo, M. *et al.* (2012) A radial glia-specific role of RhoA in double cortex formation. *Neuron*, **73**, 911–924.
36. Kiecker, C. and Lumsden, A. (2004) Hedgehog signaling from the ZLI regulates diencephalic regional identity. *Nat. Neurosci.*, **7**, 1242–1249.
37. Vieira, C., Garda, A.L., Shimamura, K. and Martinez, S. (2005) Thalamic development induced by Shh in the chick embryo. *Dev. Biol.*, **284**, 351–363.
38. Martinez-Ferre, A., Navarro-Garberi, M., Bueno, C. and Martinez, S. (2013) Wnt signal specifies the intrathalamic limit and its organizer properties by regulating Shh induction in the alar plate. *J. Neurosci.*, **33**, 3967–3980.
39. Bluske, K.K., Vue, T.Y., Kawakami, Y., Taketo, M.M., Yoshikawa, K., Johnson, J.E. and Nakagawa, Y. (2012) beta-Catenin signaling specifies progenitor cell identity in parallel with Shh signaling in the developing mammalian thalamus. *Development*, **139**, 2692–2702.
40. Kataoka, A. and Shimogori, T. (2008) Fgf8 controls regional identity in the developing thalamus. *Development*, **135**, 2873–2881.
41. Hagemann, A.I. and Scholpp, S. (2012) The Tale of the Three Brothers—Shh, Wnt, and Fgf during development of the thalamus. *Front. Neurosci.*, **6**, 76.
42. McConnell, S.K., Ghosh, A. and Shatz, C.J. (1989) Subplate neurons pioneer the first axon pathway from the cerebral cortex. *Science*, **245**, 978–982.
43. De Carlos, J.A. and O'Leary, D.D. (1992) Growth and targeting of subplate axons and establishment of major cortical pathways. *J. Neurosci.*, **12**, 1194–1211.
44. Super, H., Soriano, E. and Uylings, H.B. (1998) The functions of the preplate in development and evolution of the neocortex and hippocampus. *Brain Res. Brain Res. Rev.*, **27**, 40–64.
45. Lakhina, V., Falnikar, A., Bhatnagar, L. and Tole, S. (2007) Early thalamocortical tract guidance and topographic sorting of thalamic projections requires LIM-homeodomain gene Lhx2. *Dev. Biol.*, **306**, 703–713.
46. Piper, M., Plachez, C., Zalucki, O., Fothergill, T., Goudreau, G., Erzurumlu, R., Gu, C. and Richards, L.J. (2009) Neuropilin 1-Sema signaling regulates crossing of cingulate pioneering axons during development of the corpus callosum. *Cereb. Cortex*, **19** (Suppl 1), i11–i21.
47. Wang, C., Pan, Y. and Wang, B. (2007) A hypermorphic mouse Gli3 allele results in a polydactylous limb phenotype. *Dev. Dyn.*, **236**, 769–776.
48. Ball, G., Boardman, J.P., Rueckert, D., Aljabar, P., Arichi, T., Merchant, N., Gousias, I.S., Edwards, A.D. and Counsell, S.J. (2012) The effect of preterm birth on thalamic and cortical development. *Cereb. Cortex*, **22**, 1016–1024.
49. Hoon, A.H. Jr, Stashinko, E.E., Nagae, L.M., Lin, D.D., Keller, J., Bastian, A., Campbell, M.L., Levey, E., Mori, S. and Johnston, M.V. (2009) Sensory and motor deficits in children with cerebral palsy born preterm correlate with diffusion tensor imaging abnormalities in thalamocortical pathways. *Dev. Med. Child. Neurol.*, **51**, 697–704.
50. Baker, K., Northam, G.B., Chong, W.K., Banks, T., Beales, P. and Baldeweg, T. (2011) Neocortical and hippocampal volume loss in a human ciliopathy: a quantitative MRI study in Bardet-Biedl syndrome. *Am. J. Med. Genet. A*, **155A**, 1–8.
51. Keppler-Noreuil, K.M., Blumhorst, C., Sapp, J.C., Brinckman, D., Johnston, J., Nopoulos, P.C. and Biesecker, L.G. (2011) Brain tissue- and region-specific abnormalities on volumetric MRI scans in 21 patients with Bardet-Biedl syndrome (BBS). *BMC Med. Genet.*, **12**, 101.
52. Yun, K., Potter, S. and Rubenstein, J.L. (2001) Gsh2 and Pax6 play complementary roles in dorsoventral patterning of the mammalian telencephalon. *Development*, **128**, 193–205.
53. Bulfone, A., Puelles, L., Porteus, M.H., Frohman, M.A., Martin, G.R. and Rubenstein, J.L. (1993) Spatially restricted expression of Dlx-1, Dlx-2 (Tes-1), Gbx-2, and Wnt-3 in the embryonic day 12.5 mouse forebrain defines potential transverse and longitudinal segmental boundaries. *J. Neurosci.*, **13**, 3155–3172.
54. Wassarman, K.M., Lewandoski, M., Campbell, K., Joyner, A.L., Rubenstein, J.L., Martinez, S. and Martin, G.R. (1997) Specification of the anterior hindbrain and establishment of a normal mid/hindbrain organizer is dependent on Gbx2 gene function. *Development*, **124**, 2923–2934.
55. Hui, C.C., Slusarski, D., Platt, K.A., Holmgren, R. and Joyner, A. L. (1994) Expression of three mouse homologs of the Drosophila segment polarity gene cubitus interruptus, Gli, Gli-2, and Gli-3, in ectoderm- and mesoderm-derived tissues suggests multiple roles during postimplantation development. *Dev. Biol.*, **162**, 402–413.
56. Gradwohl, G., Fode, C. and Guillemot, F. (1996) Restricted expression of a novel murine atonal-related bHLH protein in undifferentiated neural precursors. *Dev. Biol.*, **180**, 227–241.
57. Lazzaro, D., Price, M., de Felice, M. and Di Lauro, R. (1991) The transcription factor TTF-1 is expressed at the onset of thyroid and lung morphogenesis and in restricted regions of the foetal brain. *Development*, **113**, 1093–1104.
58. Grigoriou, M., Tucker, A.S., Sharpe, P.T. and Pachnis, V. (1998) Expression and regulation of Lhx6 and Lhx7, a novel subfamily of LIM homeodomain encoding genes, suggests a role in mammalian head development. *Development*, **125**, 2063–2074.
59. Qiu, M., Shimamura, K., Sussel, L., Chen, S. and Rubenstein, J. L. (1998) Control of anteroposterior and dorsoventral domains

of Nkx-6.1 gene expression relative to other Nkx genes during vertebrate CNS development. *Mech. Dev.*, **72**, 77–88.
60. Goodrich, L.V., Johnson, R.L., Milenkovic, L., McMahon, J.A. and Scott, M.P. (1996) Conservation of the hedgehog/patched signaling pathway from flies to mice: induction of a mouse patched gene by Hedgehog. *Genes Dev.*, **10**, 301–312.
61. Echelard, Y., Epstein, D.J., St-Jacques, B., Shen, L., Mohler, J., McMahon, J.A. and McMahon, A.P. (1993) Sonic hedgehog, a member of a family of putative signaling molecules, is implicated in the regulation of CNS polarity. *Cell*, **75**, 1417–1430.
62. Theil, T. (2005) Gli3 is required for the specification and differentiation of preplate neurons. *Dev. Biol.*, **286**, 559–571.
63. Paschaki, M., Schneider, C., Rhinn, M., Thibault-Carpentier, C., Dembele, D., Niederreither, K. and Dolle, P. (2013) Transcriptomic analysis of murine embryos lacking endogenous retinoic acid signaling. *PLoS ONE*, **8**, e62274.